AIP | Journal of Applied Physics

Parametrization of the Stillinger-Weber potential for Si/N/H system and its application to simulations of silicon nitride film deposition with SiH4/NH3

Xiaodi Deng, Yixu Song, JinChun Li, and Yikang Pu

Citation: Journal of Applied Physics **115**, 054902 (2014); doi: 10.1063/1.4863841
View online: http://dx.doi.org/10.1063/1.4863841
View Table of Contents: http://scitation.aip.org/content/aip/journal/jap/115/5?ver=pdfcov
Published by the AIP Publishing

Parametrization of the Stillinger-Weber potential for Si/N/H system and its application to simulations of silicon nitride film deposition with SiH_4/NH_3

Xiaodi Deng,[1,a] Yixu Song,[2] JinChun Li,[3] and Yikang Pu[1]
[1]*Department of Engineering Physics, Tsinghua University, Beijing 100084, People's Republic of China*
[2]*State Key Laboratory on Intelligent Technology and Systems, Tsinghua National Laboratory for Information Science and Technology, Department of Computer Science and Technology, Tsinghua University, Beijing 100084, People's Republic of China*
[3]*Institute of Applied Physics, University of Science and Technology Beijing, Beijing 100083, China*

(Received 15 October 2013; accepted 17 January 2014; published online 3 February 2014)

We determined the Stillinger-Weber interatomic potential parameters for Si/N/H system based on first principles density functional calculations. This new potential can be used to perform classical molecular dynamics simulation for silicon nitride deposition on Si substrate. During the first principles calculations, cluster models have been carefully and systematically chosen to make sampling of the interatomic potential supersurface more thoroughly. Global optimization method was used to fit the *ab initio* data into Stillinger-Weber form. We used a recursive method to perform the classical molecular dynamics simulations for silicon nitride (SiN) film growth on Si substrate with SiH_4/NH_3 gas mixtures. During the simulation, we could clearly observe the silicon nitride film growth progress. In this paper, we present the details of potential derivation and simulation results with different SiH_4:NH_3 ratios. It is demonstrated that this new potential is suitable to describe the surface reactions of the Si/N/H system and allows us to explore more complex SiN growing process such as plasma-enhanced chemical vapor deposition. © *2014 AIP Publishing LLC*. [http://dx.doi.org/10.1063/1.4863841]

I. INTRODUCTION

In the microelectronic industry, silicon nitride film has been widely used and extensively investigated due to its excellent mechanical and electronic properties. To gain better control of the film quality, it is very important to understand the film growth mechanism. However, fundamental understanding of the interaction process is still incomplete.

Molecular-dynamics (MD) simulation is a very important tool to study the surface reaction for various processes in semiconductor industry, including reactive ion etching (RIE)[1,2] and plasma-enhanced chemical vapor deposition (PECVD). Comparing with *ab initio* MD simulations, classic MD simulations benefit both on scales of simulation time and particle numbers. The construction of a potential model is one of the most important issues for performing classic MD simulations.

For simulations involving Si atoms, several potential models have been proposed. First, Stillinger and Weber (SW) developed a potential model with two-body and three-body functions for Si and F systems.[3–6] This model was then modified and improved to obtain much better simulation results. Parameter sets for various systems (Si/F,[3–5,7] Si/Cl,[8,9] Si/O,[10–13] Si/O/F, Si/O/Cl,[14] Si/O/C/F,[15] Si/O/C/H,[16] Si/Br,[17] and Si/Br/H[18]) have been determined based on experimental data or first principle calculations. Then, based on the concept of bond order, Tersoff proposed another widely used potential which includes multi-body interactions.[19] This model was mostly used for systems containing C atoms including Si,[19–21] C,[22] Si/C,[23] C/H,[24] C/F,[25] and Si/C/F.[26]

In recent years, the development of SW potential is in two main directions. First, the reparametrizations of the original parameter sets to make them more suitable to certain problems. Pizzagalli *et al.*[27] developed new parameter sets for silicon, which can improve the description of defects and plasticity-related properties. Lee *et al.*[28] used a force-matching method to optimize the parameters of SW potential for calculation of the lattice thermal conductivity of silicon. In addition to these parameter set refinements, the form of the SW model has also been slightly modified. Ohta *et al.*[29] added a new parameter to the three-body term of the SW potential, which made the new model having better effect for reactive ion etching simulations in Si/halogen systems. The other direction includes developing parameter sets for new systems. Ohta *et al.*[17] reported a new parameter set for Si/Br system and Nagaoka *et al.*[18] then extended it to include H atoms.

In order to have better understanding of silicon nitride film growth process at atomic level, we developed a new potential model for Si/N/H system by parametrizing the widely used SW-type potential. In this paper, we present the details of parametrization process by using data from *ab initio* first principles density functional calculations. Classic MD simulations of silicon nitride film growth on Si substrate with SiH_4/NH_3 gas mixture are also reported.

II. SW-TYPE POTENTIAL FUNCTIONS

In SW-type potential model, the total energy of an atomic system is the summation of a two-body term and a three-body term.[3–5]

$$\Phi = \sum_{i<j} v_2(i,j) + \sum_{i<j<k} v_3(i,j,k). \quad (1)$$

[a]Electronic mail: dixiaodeng@gmail.com

The two-body part which describes the pairlike interaction between the ith and the jth atoms is given by

$$v_2(i,j) \equiv f_2^{ij}(r_{ij}) = A_{ij}(B_{ij}r_{ij}^{-p_{ij}} - r_{ij}^{-q_{ij}})\exp\left[\frac{1}{r_{ij}-a_{ij}}\right], \quad (2)$$

if $r_{ij} < a_{ij}$ and $v_2(i,j) = 0$ otherwise. In Eq. (2), $r_{ij} = |\mathbf{r}_i - \mathbf{r}_j|$ denotes the distance between the ith and the jth atom located at $\mathbf{r}_i$ and $\mathbf{r}_j$. A_{ij}, B_{ij}, p_{ij}, q_{ij}, and a_{ij} are parameters that depend on the element types of the ith and the jth atoms. Parameters A_{ij}, B_{ij}, p_{ij}, and a_{ij} are all positive. The function automatically cuts off at $r_{ij} = a_{ij}$. Considering system symmetry, all these parameters should be invariant when the indices i and j are exchanged, i.e., $A_{ij} = A_{ji}$, $B_{ij} = B_{ji}$,…, etc.

The three-body term is a summation of three parts

$$v_3(i,j,k) \equiv f_3^{ijk}(\mathbf{r}_i,\mathbf{r}_j,\mathbf{r}_k) = h_{jik}(r_{ij},r_{ik},\theta_{jik}) + h_{ijk}(r_{ji},r_{jk},\theta_{ijk}) + h_{ikj}(r_{ki},r_{kj},\theta_{ikj}), \quad (3)$$

where θ_{jik} is the angle between vectors $\mathbf{r}_{ij} = \mathbf{r}_j - \mathbf{r}_i$ and $\mathbf{r}_{ik} = \mathbf{r}_k - \mathbf{r}_i$ at vertex $\mathbf{r}_i$. h_{ijk} is given by either

$$h_{jik}(r,s,\theta) = \lambda_{jik}\exp\left[\frac{\gamma_{jik}^{j}}{r-a_{jik}^{j}} + \frac{\gamma_{jik}^{k}}{s-a_{jik}^{k}}\right] \quad (4)$$

or

$$h_{jik}(r,s,\theta) = \lambda_{jik}\exp\left[\frac{\gamma_{jik}^{j}}{r-a_{jik}^{j}} + \frac{\gamma_{jik}^{k}}{s-a_{jik}^{k}}\right] \times |\cos\theta - \cos\theta_{jik}^{0}|^2, \quad (5)$$

if $r < a_{jik}^{j}$ and $s < a_{jik}^{k}$ and $h_{jik}(r,s,\theta) = 0$ otherwise, depending on the element type of the ith atom. In Eqs. (4) and (5), λ_{jik}, γ_{jik}^{j}, γ_{jik}^{k}, a_{jik}^{j}, a_{jik}^{k}, θ_{jik}^{0} are parameters that depend on the species of the (i, j, k) triplet. The cut-off distances are denoted by a_{jik}^{j} and a_{jik}^{k}, while θ_{jik}^{0} is the desired interbond angle. Parameters λ_{jik}, γ_{jik}^{j}, γ_{jik}^{k}, a_{jik}^{j}, and a_{jik}^{k} are positive and $0^\circ < \theta_{jik}^{0} < 180^\circ$. The system symmetry requires the invariance of these parameters under the exchange of the first and the third indices, i.e., $\lambda_{jik} = \lambda_{kij}$, $\gamma_{jik} = \gamma_{kij}$,…, etc.

III. PARAMETER FITTING

A. *Ab initio* calculations

As proposed by Ohta *et al.*,[17] the interatomic forces can be obtained from the derivatives of the interatomic potential functions with respect to the positions of the nucleus. Therefore, in our study, all the computational models are based on simple atoms rather than complex compound clusters. The calculations were performed using the density functional theory (DFT) that has been implemented in Vienna *ab initio* simulation package (VASP).[30,31] For the exchange-correlation functional, we used the PW91 (Refs. 32 and 33) version of the generalized gradient approximation (GGA).

Computational models for two-body function and three-body function parameter fittings are quite different. The atomic configurations and processing of the obtained data for both kinds of functions are discussed in detail in Secs. III B–III D.

B. Two-body functions

Parameters for two-body functions and three-body functions were determined separately and independently. First, we determined parameters for the two-body functions. There are six two-body pairs for Si/N/H system, which are Si–Si, Si–N, Si–H, N–N, N–H, and H–H. For the Si–Si pair, the original parameters were used without further modification.[3] The *ab initio* data of the other five pairs were obtained from calculations carried out on the two-atom clusters i–j (i,j = Si, N, H) by varying the bond lengths. For the H–H pair, none spin polarized calculations were performed, while for Si–H, N–N, and N–H pairs spin polarized calculations were performed. The energy summation of two isolated atoms was considered as the zero reference for the clusters. Specifically, Eq. (6) was used to calculate the potential energy for parameter fitting of cluster i–j.

$$v_2(i,j) = E_{ij} - (E_i + E_j), \quad (6)$$

where i,j = Si, N, H.

Fig. 1 shows the *ab initio* data points and the fitted curves of the two-body functions. The parameters A_{ij}, B_{ij}, p_{ij}, q_{ij}, and a_{ij} are summarized in Table I. In Table II, we list the bond lengths and bond energies calculated with these optimized fitting parameters compared to experimental data. Overall, the results obtained with our parameters are in good agreement with the experimental data.

C. Three-body functions

Next, we determined parameters for three-body functions. There are 27 triple combinations for Si/N/H system. System symmetry requires that the parameters are invariant when the indexes of the first atom and the third atom are

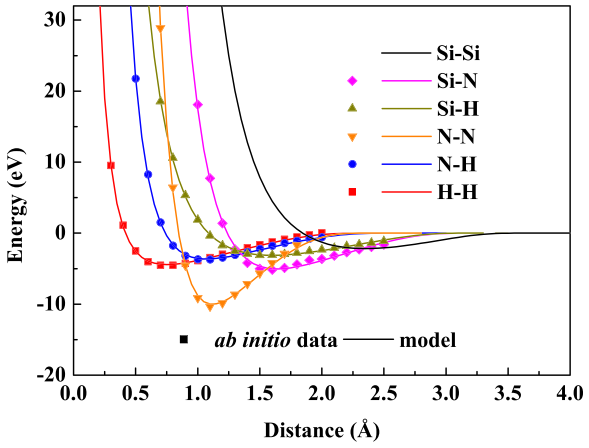

FIG. 1. Parameter fitting for two-body functions. Scatter points are data from the *ab initio* calculations and solid lines are plots of two-body functions with the optimized fitting parameters.

TABLE I. SW parameter sets for the Si/N/H system.

v_2(H,H)[a]	$A_{HH} = 80.3919$ $B_{HH} = 0.8556$ $p_{HH} = 1.2534$ $q_{HH} = 1.1567$ $a_{HH} = 2.5141$	v_2(N,H)[a]	$A_{NH} = 37.8863$ $B_{NH} = 0.7267$ $p_{NH} = 2.0240$ $q_{NH} = 1.7181$ $a_{NH} = 2.7236$	v_2(Si,H)[a]	$A_{SiH} = 92.4289$ $B_{SiH} = 0.8742$ $p_{SiH} = 1.6222$ $q_{SiH} = 1.4173$ $a_{SiH} = 3.3522$
v_2(N,N)[a]	$A_{NN} = 125.3646$ $B_{NN} = 0.7355$ $p_{NN} = 2.5362$ $q_{NN} = 2.1976$ $a_{NN} = 2.5141$	v_2(Si,N)[a]	$A_{SiN} = 105.0668$ $B_{SiN} = 0.8301$ $p_{SiN} = 2.5718$ $q_{SiN} = 2.2178$ $a_{SiN} = 3.3522$	v_2(Si,Si)[a]	$A_{SiSi} = 15.2952$ $B_{SiSi} = 0.6022$ $p_{SiSi} = 4.0$ $q_{SiSi} = 0$ $a_{SiSi} = 3.7712$
h(H,H,H)[b]	$\lambda_{HHH} = 20.0591$ $\gamma^{H}_{HHH} = 1.4689$ $a^{H}_{HHH} = a_{HH}$	h(N,N,N)[b]	$\lambda_{NNN} = 178.2324$ $\gamma^{N}_{NNN} = 2.0628$ $a^{N}_{NNN} = a_{NN}$	h(Si,Si,Si)[c]	$\lambda_{SiSiSi} = 45.5628$ $\gamma^{Si}_{SiSiSi} = 2.5141$ $a^{Si}_{SiSiSi} = a_{SiSi}$ $\theta^{0}_{SiSiSi} = 109.4712$
h(H,N,N)[b]	$\lambda_{HNN} = 24.0330$ $\gamma^{H}_{HNN} = 2.2849$ $\gamma^{N}_{HNN} = \gamma^{N}_{NNN}$ $a^{H}_{HNN} = a_{NH}$ $a^{N}_{HNN} = a_{NN}$	h(N,N,H)[b]	$\lambda_{NNH} = 59.8702$ $\gamma^{N}_{NNH} = \gamma^{N}_{NNN}$ $\gamma^{H}_{NNH} = \gamma^{H}_{HNN}$ $a^{H}_{NNH} = a_{NH}$ $a^{N}_{NNH} = a_{NN}$	h(H,Si,Si)[b]	$\lambda_{HSiSi} = 24.2071$ $\gamma^{H}_{HSiSi} = 5.0$ $\gamma^{Si}_{HSiSi} = \gamma^{Si}_{SiSiSi}$ $a^{H}_{HSiSi} = a_{SiH}$ $a^{Si}_{HSiSi} = a_{SiSi}$
h(Si,Si,H)[c]	$\lambda_{SiSiH} = 12.660$ $\gamma^{H}_{SiSiH} = \gamma^{H}_{HSiSi}$ $\gamma^{Si}_{SiSiH} = \gamma^{Si}_{SiSiSi}$ $a^{H}_{SiSiH} = a_{SiH}$ $a^{Si}_{SiSiH} = a_{SiSi}$ $\theta^{0}_{SiSiH} = 109.471$	h(N,H,H)[c]	$\lambda_{NHH} = 20.0144$ $\gamma^{H}_{NHH} = \gamma^{H}_{HHH}$ $\gamma^{N}_{NHH} = 1.083$ $a^{H}_{NHH} = a_{HH}$ $a^{N}_{NHHN} = a_{NH}$ $\theta^{0}_{NHH} = 107.18$	h(H,H,N)[b]	$\lambda_{HHN} = 1.8668$ $\gamma^{H}_{HHN} = \gamma^{H}_{HHH}$ $\gamma^{N}_{HHN} = \gamma^{N}_{NHH}$ $a^{H}_{HHN} = a_{HH}$ $a^{N}_{HHN} = a_{NH}$
h(N,Si,Si)[c]	$\lambda_{NSiSi} = 20.8330$ $\gamma^{N}_{NSiSi} = 2.0951$ $\gamma^{Si}_{NSiSi} = \gamma^{Si}_{SiSiSi}$ $a^{N}_{NSiSi} = a_{SiN}$ $a^{Si}_{NSiSi} = a_{SiSi}$ $\theta^{0}_{NSiSi} = 120.0$	h(Si,Si,N)[c]	$\lambda_{SiSiN} = 9.4510$ $\gamma^{N}_{SiSiN} = \gamma^{N}_{NSiSi}$ $\gamma^{Si}_{SiSiN} = \gamma^{Si}_{SiSiSi}$ $a^{N}_{SiSiN} = a_{SiN}$ $a^{Si}_{SiSiN} = a_{SiSi}$ $\theta^{0}_{SiSiN} = 111.147$	h(*Si*,*H*,*H*)[c]	$\lambda_{SiHH} = 6.1158$ $\gamma^{H}_{SiHH} = \gamma^{H}_{HHH}$ $\gamma^{Si}_{SiHH} = 1.1012$ $a^{H}_{SiHH} = a_{HH}$ $a^{Si}_{SiHH} = a_{SiH}$ $\theta^{0}_{SiHH} = 110.0$
h(H,H,Si)[b]	$\lambda_{HHSi} = 5.9193$ $\gamma^{H}_{HHSi} = \gamma^{H}_{HHH}$ $\gamma^{Si}_{HHSi} = \gamma^{Si}_{SiHH}$ $a^{H}_{HHSi} = a_{HH}$ $a^{Si}_{HHSi} = a_{SiH}$	h(Si,N,N)[c]	$\lambda_{SiNN} = 14.7853$ $\gamma^{N}_{SiNN} = \gamma^{N}_{NNN}$ $\gamma^{Si}_{SiNN} = 1.8242$ $a^{N}_{SiNN} = a_{NN}$ $a^{Si}_{SiNN} = a_{SiN}$ $\theta^{0}_{SiNN} = 112.0$	h(N,N,Si)[b]	$\lambda_{NNSi} = 62.8817$ $\gamma^{N}_{NNSi} = \gamma^{N}_{NNN}$ $\gamma^{Si}_{NNSi} = \gamma^{Si}_{SiNN}$ $a^{N}_{NNSi} = a_{NN}$ $a^{Si}_{NNSi} = a_{SiN}$
h(Si,N,H)[c]	$\lambda_{SiNH} = 3.0484$ $\gamma^{H}_{SiNH} = \gamma^{Si}_{SiHH}$ $\gamma^{N}_{SiNH} = \gamma^{Si}_{SiNN}$ $a^{H}_{SiNH} = a_{SiH}$ $a^{N}_{SiNH} = a_{SiN}$ $\theta^{0}_{SiNH} = 134.09$	h(N,H,Si)[c]	$\lambda_{NHSi} = 7.8845$ $\gamma^{H}_{NHSi} = \gamma^{N}_{NHH}$ $\gamma^{Si}_{NHSi} = \gamma^{N}_{NSiSi}$ $a^{H}_{NHSi} = a_{NH}$ $a^{Si}_{NHSi} = a_{SiN}$ $\theta^{0}_{NHSi} = 120.0$	h(H,Si,N)[b]	$\lambda_{HSiN} = 1.1738$ $\gamma^{Si}_{HSiN} = \gamma^{H}_{HSiSi}$ $\gamma^{N}_{HSiN} = \gamma^{H}_{HNN}$ $a^{Si}_{HSiN} = a_{SiH}$ $a^{N}_{HSiN} = a_{NH}$

[a]Equation (2).
[b]Equation (4).
[c]Equation (5).

exchanged. With this in consideration, parameters for only 18 triplets would be determined.

The data used to determine parameters for the three-body functions were obtained by performing first-principles calculations on three-atom clusters. Fig. 2 shows the model used for the calculations. The *ab initio* data were obtained by scanning bond lengths r_{ij}, r_{jk}, and r_{ik}. The scanning range for the bond lengths was chosen carefully to make sure that interactions between the atoms are the most effective. Table III lists the scanning ranges of the six kinds of bond pairs for the Si/N/H system. The scanning step was 0.2 Å. The zero reference for the three-atom cluster was considered to be the summation of the energies of the three isolated atoms in the cluster. Therefore, the *ab initio* potential energy data for the three-atom cluster can be calculated from the following equation:

$$\Phi(i,j,k) = E_{ijk} - (E_i + E_j + E_k). \quad (7)$$

TABLE II. Bond lengths (r) and bond energies (E) calculated from two-body functions using the optimized fitting parameters as compared to experimental data.

	r(Å)		E(eV)	
Bond	This work	Expt.	This work	Expt.
Si–Si	2.35	2.17	…	…
Si–N	1.64	1.57[a]	5.04	4.87[a]
Si–H	1.60	1.52[a]	3.12	3.10[a]
N–N	1.12	1.10[a]	10.02	9.80[a]
N–H	1.07	1.04[a]	3.64	3.51[a]
H–H	0.75	0.74[a]	4.42	4.52[a]

[a]Reference 34.

The *ab initio* data obtained from these three-atom clusters can be used to fit the SW function Eq. (1), which is the sum of two-body terms and three-body terms. During the parameter fittings, we used Eq. (5) for the triplets, which can form stable bond angles while using Eq. (4) for the others. More specifically, for triplets (i,j,k) we use Eq. (5) when $i=$ Si, N and we used Eq. (4) when $i=$ H. Exceptions were made for N–N–N cluster, for which Eq. (4) was used instead. To keep things simple, the cut-off distance parameters in Eqs. (4) and (5) were extended from the pre-determined two-body functions.[3] Therefore, we had $a^j_{ijk}=a_{ij}$ and $a^k_{jik}=a_{ik}$. The other parameters λ_{jik}, γ^j_{jik}, γ^k_{jik} in Eq. (4) and λ_{jik}, γ^j_{jik}, γ^k_{jik}, θ^0_{jik} in Eq. (5) would be determined in parameter fittings by global optimization method.

To systematically determine all parameters for the total 18 triplets of Si/N/H system, we decided to divide them into three types: *A–A–A* type, *A–B–B* type, and *A–B–C* type. This kind of grouping strategy resulted in 10 independent three-atom configurations (or *ab initio* data sets) based on which we did the parameter fittings. When considering that the major role of three-body function (3) is to cancel the attractions resulting from the simple summation of two-body terms,[4,29] some assumptions could be made to make the parameter determination simpler. For instance, the results of

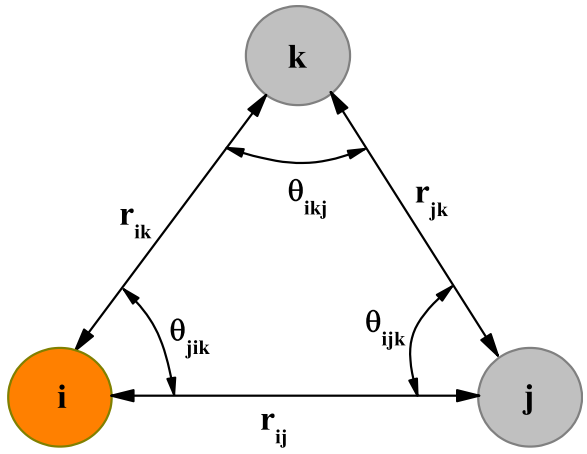

FIG. 2. Cluster model which was used for first principles calculation to obtain *ab initio* data for three-body function parameter fitting. Bond lengths r_{ij}, r_{ik}, and r_{jk} were scanned to sample the potential energy surface.

TABLE III. Bond length scanning ranges for the three-atom cluster models.

Bond	Range (Å)
Si–Si	1.5–3.0
Si–N	0.8–2.0
Si–H	0.8–2.8
N–N	0.8–2.0
N–H	0.8–2.0
H–H	0.3–2.0

A–A–A type could be used by *A–B–B* type whose results could be further used by *A–B–C* type. Therefore, parameter determination for these three types was in the following order: *A–A–A*, *A–B–B*, and *A–B–C*. Details about the three-body function parameter fitting for each type are discussed in the Subsections III C 1–III C 3. Fitting errors for each cluster model are listed in Table IV and all the fitted parameters are summarized in Table I. For data sets which involved Si-N bonds, the absolute maximum fitting errors $\Delta\Phi_{max}$ were higher than the others. It was because that the absolute potential energy was higher for these data sets. However, when considering the relative errors or the agreement factor of the parameter fitting R, they were all in the acceptable ranges (<0.05).

1. A–A–A type

There are three *A–A–A* type triplets: Si–Si–Si, N–N–N, and H–H–H. For Si–Si–Si, the original three-body parameters were used without further modification.[3] Therefore, only the parameters of H–H–H and N–N–N were fitted. Here, H–H–H is used to illustrate how the parameters of three-body function were determined for this type of triplets. The parameters for N–N–N were determined using the same method.

We used Eq. (4) for H–H–H. Obviously, *A–A–A* type triplets have the property that $i\equiv j\equiv k$ in Eq. (4). As a result, the γ parameters in Eq. (4) are equivalent. Additionally, we had $a^H_{HHH}=a_{HH}$. Therefore, the parameters needed to model H–H–H three-body function were reduced to only two: λ_{HHH} and γ^H_{HHH}. Model function (8) was used to fit the *ab initio* data for *H–H–H*

TABLE IV. Fitting errors between the SW potential model function and the *ab initio* data for each three-atom configuration. $\Delta\Phi_{max}$ is the maximum and $\Delta\Phi_{avg}$ is the average value of the fitting residuals, R is the agreement factor of the parameter fitting defined as $R=\Sigma(\Phi_{model}-\Phi_{ab\,initio})^2/\Sigma(\Phi_{ab\,initio})^2$.

Data set	$\Delta\Phi_{max}$(eV)	$\Delta\Phi_{avg}$(eV)	R
(H, H, H)	0.837	0.059	0.010
(N, N, N)	1.532	0.065	0.006
(Si, Si, Si)	…	…	…
(H, N, N)	1.502	−0.021	0.017
(H, Si, Si)	2.752	−0.146	0.045
(N, H, H)	5.166	−0.062	0.026
(N, Si, Si)	7.864	0.111	0.006
(Si, H, H)	3.715	−0.064	0.012
(Si, N, N)	6.757	0.277	0.007
(Si, N, H)	3.032	−0.043	0.006

$$\Phi(H,H,H) = f_2^{HH}(r_{ij}) + f_2^{HH}(r_{ik}) + f_2^{HH}(r_{jk}) + \lambda_{HHH}\exp\left[\frac{\gamma_{HHH}^{H}}{r_{ij}-a_{HH}} + \frac{\gamma_{HHH}^{H}}{r_{ik}-a_{HH}}\right] + \lambda_{HHH}\exp\left[\frac{\gamma_{HHH}^{H}}{r_{ij}-a_{HH}} + \frac{\gamma_{HHH}^{H}}{r_{jk}-a_{HH}}\right] + \lambda_{HHH}\exp\left[\frac{\gamma_{HHH}^{H}}{r_{ik}-a_{HH}} + \frac{\gamma_{HHH}^{H}}{r_{jk}-a_{HH}}\right]. \quad (8)$$

The fitting errors are listed in Table IV and all the determined parameters for *A–A–A* type triplets are listed in Table I.

2. A–B–B type

There are six *A–B–B* type triplet configurations for Si/N/H system. Each triplet configuration of *A–B–B* type triplets contains three concrete triplets: *A–B–B*, *B–B–A*, and *B–A–B*. However, the latter two triplets are symmetry equivalent and they have exactly the same parameters. Therefore, each triplet configuration corresponds to only two independent triplets. When one triplet contains more than one kind of atoms, we decided that for parameters γ we used the results of *A–A–A* types when the two-body portion of Eq. (4) or Eq. (5) represents the same kind of atoms. As a result, we had $\gamma_{ijj}^{j} \equiv \gamma_{jji}^{j} \equiv \gamma_{jjj}^{j}$. During the parameters fittings, constrains were applied to bond angles to make them varying in reasonable ranges. Here, we use Si–N–N as an example to illustrate the procedure of parameter fitting for *A–B–B* type, parameters for the other five groups were determined using the same method.

To build the SW model function for Si–N–N, we used Eq. (5) for h_{SiNN} and Eq. (4) for h_{NNSi}. Here, h_{NNSi} and h_{NSiN} were equivalent. Using the same simplification for parameter γ and cut-off distance a discussed in the above sections, we had $\gamma_{NNSi}^{N} \equiv \gamma_{NSiN}^{N} \equiv \gamma_{NNN}^{N}$, $\gamma_{NNSi}^{N} \equiv \gamma_{NSiN}^{N}$, $\gamma_{NNSi}^{Si} \equiv \gamma_{NSiN}^{Si}$, $a_{SiNN}^{Si} = a_{SiN}$, $a_{NNSi}^{N} \equiv a_{NSiN}^{N} = a_{NN}$, $a_{NNSi}^{Si} \equiv a_{NSiN}^{Si} = a_{SiN}$. With all these considerations, we had the model function (9), which was used to fit the *ab initio* data calculated for Si–N–N cluster. The fitting errors are listed in Table IV and the obtained parameters are listed in Table I.

$$\Phi(Si,N,N) = f_2^{SiN}(r_{ij}) + f_2^{SiN}(r_{ik}) + f_2^{NN}(r_{jk}) + \lambda_{SiNN}\exp\left[\frac{\gamma_{SiNN}^{Si}}{r_{ij}-a_{SiN}} + \frac{\gamma_{SiNN}^{Si}}{r_{ik}-a_{SiN}}\right] \times |\cos\theta_{jik} - \cos\theta_{SiNN}^{0}|^2 + \lambda_{NNSi}\exp\left[\frac{\gamma_{NNSi}^{Si}}{r_{ij}-a_{SiN}} + \frac{\gamma_{NNN}^{N}}{r_{jk}-a_{NN}}\right] + \lambda_{NNSi}\exp\left[\frac{\gamma_{NNSi}^{Si}}{r_{ik}-a_{SiN}} + \frac{\gamma_{NNN}^{N}}{r_{jk}-a_{NN}}\right]. \quad (9)$$

3. A–B–C type

There is only one *A–B–C* type triplet configuration for Si/N/H system. It contains three pairs of symmetry equivalent triplets. As discussed in the above two sections, when building the fitting function, the γ parameters in these triplets are replaced with the corresponding *A–B–B* type parameters. In this case, we have $\gamma_{SiNH}^{N} \equiv \gamma_{SiNN}^{Si}$, $\gamma_{SiNH}^{H} \equiv \gamma_{SiHH}^{Si}$, $\gamma_{NHSi}^{H} \equiv \gamma_{NHH}^{N}$, $\gamma_{NHSi}^{Si} \equiv \gamma_{NSiSi}^{N}$, $\gamma_{HSiN}^{S} i \equiv \gamma_{HSiSi}^{H}$, $\gamma_{HSiN}^{N} \equiv \gamma_{HNN}^{H}$. Then, we can write down the fitting function (10) for Si–N–H

$$\Phi(Si,N,H) = f_2^{SiN}(r_{ij}) + f_2^{SiH}(r_{ik}) + f_2^{NH}(r_{jk}) + \lambda_{SiNH}\exp\left[\frac{\gamma_{SiNN}^{Si}}{r_{ij}-a_{SiN}} + \frac{\gamma_{SiHH}^{Si}}{r_{ik}-a_{SiH}}\right] \times |\cos\theta_{jik} - \cos\theta_{SiNH}^{0}|^2 + \lambda_{NHSi}\exp\left[\frac{\gamma_{SiNN}^{Si}}{r_{ij}-a_{SiN}} + \frac{\gamma_{NHH}^{N}}{r_{jk}-a_{NH}}\right] \times |\cos\theta_{ijk} - \cos\theta_{NHSi}^{0}|^2 + \lambda_{HSiN}\exp\left[\frac{\gamma_{SiHH}^{Si}}{r_{ik}-a_{SiH}} + \frac{\gamma_{NHH}^{N}}{r_{jk}-a_{NH}}\right]. \quad (10)$$

The fitted parameters (λ_{SiNH}, λ_{NHSi}, λ_{HSiN}, θ_{SiNH}^{0}, θ_{NHSi}^{0}) are listed in Table I and the fitting errors are listed in Table IV.

D. Discussion about the potential

Properties of small molecules have been calculated using our potentials and the results were compared to the experimental and *ab initio* calculations in Table V. Overall, the results were in good agreement with the experimental and theoretical data. Our potential can keep the geometry structures of the molecules very well.

In Fig. 3, we calculated the energy-versus-volume data for the three known Si_3N_4 phases: α-Si_3N_4, β-Si_3N_4, and cubic Si_3N_4 (c-Si_3N_4). The data were fitted to Birch-Murnaghan[38] equation-of-state equation (EOS) function. Fig. 3 gives the

TABLE V. Properties for small molecules calculated using this potential as compared to experimental data and *ab initio* calculations. Bond lengths r are in Å, bond energies E are in eV. Bond angles are θ.

	This work	Expt./theory
SiH_4		
r_{Si-H}	1.60 Å	1.48 Å[a]
E_{Si-H}	3.12 eV	3.42 eV[a]
θ_{H-Si-H}	109.47°	109.5°[a]
SiH_3		
r_{Si-H}	1.60 Å	1.48 Å[a]
E_{Si-H}	3.12 eV	3.25 eV[a]
θ_{H-Si-H}	110.0°	110.5°[a]
NH_3		
r_{N-H}	1.02 Å	1.028 Å[b]
θ_{H-N-H}	106.19°	106.4°[b]
$H_2Si(NH_2)_2$		
r_{Si-H}	1.58 Å	1.4807 Å[c]
r_{Si-N}	1.63 Å	1.7162 Å[c]
r_{N-H}	1.02 Å	0.9991 Å[c]
H_3SiNH_2		
r_{Si-H}	1.54 Å	1.4824 Å[c]
r_{Si-N}	1.73 Å	1.7243 Å[c]
r_{N-H}	1.09 Å	0.9980 Å[c]
θ_{Si-N-H}	106.27°	120.6°[c]

[a]Reference 35.
[b]Reference 36.
[c]Reference 37.

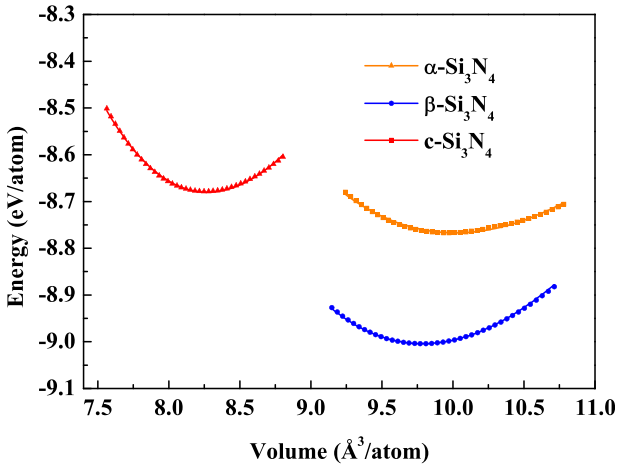

FIG. 3. Energy-volume data for three Si_3N_4 phases. Data points are calculated data using our potential model and the solid lines are fits of the Birch-Murnaghan[38] equation-of-state equation.

same phase stability trends to other *ab initio* calculation or experimental results.[39,40] Because our potential model was fitted based on single atomic configurations and omitted the corresponding crystal structure information, some of the crystal properties such as bulk module, a/c ratio that were obtained using this potential were not very ideal. Usage of this potential in these situations must be very cautious. However, it has been proved that potentials fitted using this technique perform very well for surface related simulations such as etching and deposition.[17,18] Development of this technique is needed to make it have a wider range of applications.

IV. SIMULATION OF SiH_4/NH_3 DEPOSITION ON Si SUBSTRATE

Our potential was employed to simulate silicon nitride film growth on Si substrate using SiH_4 and NH_3 gases. All simulations were performed using LAMMPS (Large-scale Atomic/Molecular Massively Parallel Simulator) code.[41] The substrate was modeled by Si (100) slab (12.288 nm × 12.288 nm) with thickness of about 30 Å. The whole structure contained about 23 552 Si atoms. During the simulation, the bottom layers of about 7.5 Å were held fixed to represent the bulk lattice. To layers about 10 Å above the fixed lattice, a thermostat was applied to simulate the substrate with constant temperature. The rest of the layers were evolved without constrains to represent the chemical reaction area. Above the substrate surface was the gas region, in which a relatively constant temperature of the gas atmosphere was maintained with thermal bath. With this basic configuration, the silicon nitride film growth was simulated by a recursive process with the following steps:

1. Add the SiH_4 and NH_3 gas mixture to the system about 10 Å above the substrate. The gas mixture was generated by randomly placing SiH_4 and NH_3 molecules with certain SiH_4:NH_3 ratio. Both temperatures of the substrate and the gases were maintained to be 900 °C.
2. Perform a long run (10 ps) on the whole system. The time step was 0.25 fs. During this step, the gases will completely react with the substrate surface.
3. Remove the atoms, molecules, and atomic clusters remained in the gas region. When one deposition cycle was finished, the product of the first two steps was used as the new substrate and the start point of the next cycle.
4. Go to step 1.

This removal and rescaling strategy resulted in an effect on accelerated deposition process. Therefore, the total simulation time was not comparable with the real situations. Although this technique neglects some atomic reactions in long time scale, we still believed that it was a good approximation of the real reaction process. Using this simulation technique, we studied the film growth process of SiH_4/NH_3 gas mixture on Si(100) substrate and the influence of different SiH_4:NH_3 ratios on the deposition results.

Fig. 5 shows a typical surface evolution with the increment of deposition cycles. The SiH_4:NH_3 ratio for simulation analyzed here is 1:20. At early stage of the deposition, NH_3 were adsorbed on the Si surface and the release of hydrogen and H atom was observed. As shown in Fig. 4, they tended to form bridge-bonded N or NH structures and this was consistent with the results of experiment and first principle studies.[42,43] When the deposition went on, small Si/N islands began to form. After that NH_3 depositions were more likely to happen at the edge of these islands. This was the same trend as reported by Dai *et al.*,[44] who studied the N insertion behavior on step-edged H/Si surfaces. As deposition went on, the Si/N islands grew continuously until they covered the Si surfaces and a "monolayer" would be formed.

When the deposition finished, silicon nitride film was formed. Fig. 6 shows the structure of the film. Totally, they were complex Si-N "networks" and the films were amorphous. However, when examined closely, the Si-N "networks" have local α-Si_3N_4 and β-Si_3N_4 micro-structures (Fig. 7). This is consistent with the fact that α and β phases have similar physical and chemical properties and are usually found to coexist during different synthesis routes.[45] The composition of the deposition layer was analyzed and plotted in Fig. 8. When the deposition began, there were a huge amount of Si dangling bonds on the substrate surface, which lowered down the H diffusion barrier. As a result, the absorption of H atoms became very easy and a drastic

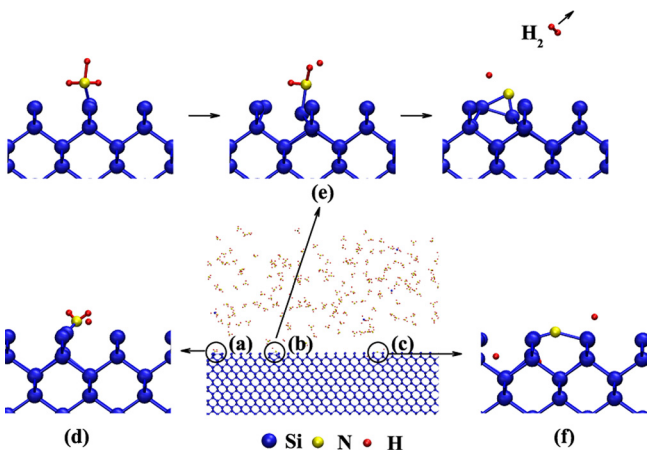

FIG. 4. Snap shots of surface evolution after different cycles of deposition viewed from the top. The SiH_4:NH_3 ratio for this simulation is 1:20.

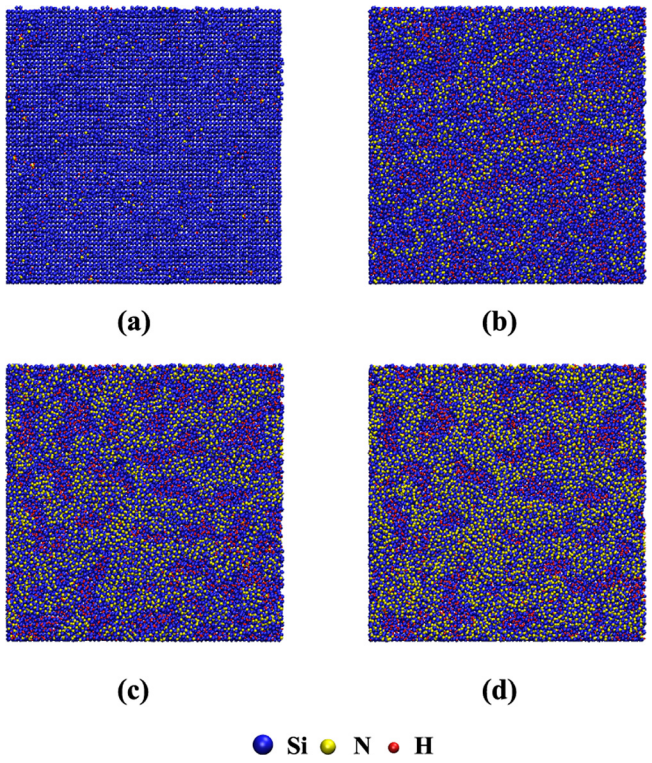

FIG. 5. Snap shot of surface structures at early stage of the deposition. (a) and (d) are NH_3 absorption on Si substrate. (b) and (e) illustrate the formation of the NH bridge-bonded structure and the releasing of hydrogen. (c) and (f) are the N bridge-bonded structure. The SiH_4:NH_3 ratio for this simulation is 1:20.

increment of H atoms at the first few deposition cycles was observed. After about 10 cycles of deposition, most of the dangling bonds were saturated and a dynamic balance was achieved for H atom absorption. In later deposition cycles, we could barely see any increments of H atoms. When the dangling bonds of Si were saturated, the deposition became stable. The Si and N atoms in the deposition layers increased linearly. At the end of the simulation, a nearly constant ratio of Si:N can be obtained.

In order to study the influence of gas mixture, simulations with different SiH_4:NH_3 ratios 1:1, 1:10, 1:20, 1:50, and 1:100 were performed. After 60 cycles of depositions, we calculated the Si:N ratio in the deposition layers and the concentration of H atoms in the reaction regions. The results are listed in Table VI. Because hydrogen has a preference to bind to silicon rather than to nitrogen,[35] and also that dangling bonds in an amorphous Si create deep states and become active for hydrogen or fluorine terminations,[46] the H concentration was usually high during the deposition. The concentration values are in the range of experiment results, which was reported to be 10%–35% typically and can be up to 40%.[35,47] Fig. 6 shows that there were few Si or N dangling bonds in the deposition layers in our simulations. Therefore, hydrogen was mostly trapped in the Si layers during the simulations. The H concentration is also slightly related with the Si_4:NH_3 ratios. When the SiH_4:NH_3 ratio was 1:1, there were barely any SiN film formed (very high Si:N ratio). This made more H atoms to be trapped by Si. As a result, the H concentration for this simulation was much higher than the others. Furthermore, SiH_4 brought more H inputs than NH_3 and this explains why the H concentration decreases when the SiH_4 portion in the gas mixture decreases (higher SiH_4:NH_3 ratio). This is the same trend to the results

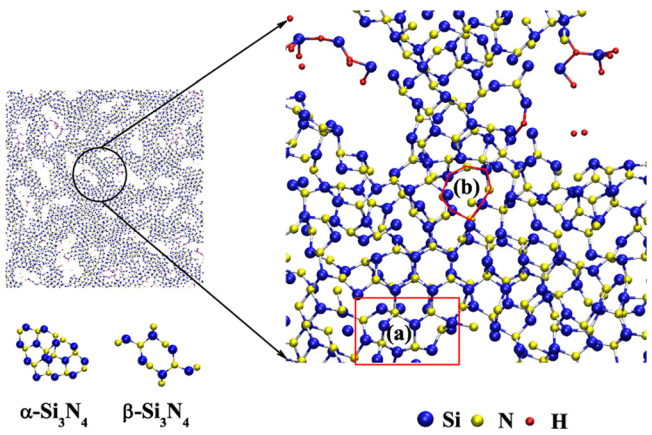

FIG. 6. Si-N film structure formed in the simulations. They are amorphous and locally having α-Si_3N_4 and β-Si_3N_4 micro-structures. (a) Local α-Si_3N_4 micro-structure. (b) Local β-Si_3N_4 micro-structure.

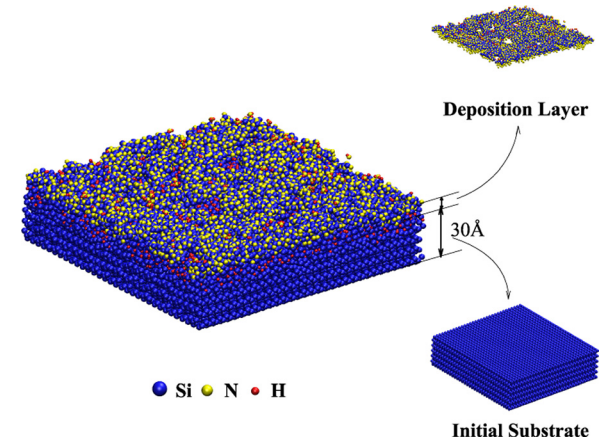

FIG. 7. Illustration of deposition layers used to analyze the film composition. Atoms above the initial substrate were treated as parts of the deposition film.

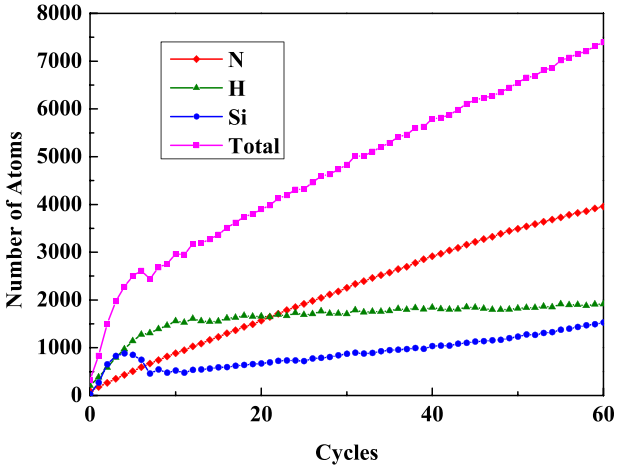

FIG. 8. The growth of number of atoms for N, H, and Si in the deposition layer with the deposition cycles. The SiH_4:NH_3 ratio for this simulation is 1:20.

TABLE VI. Si:N ratio in the deposited layers, H atomic concentration in the chemical reaction region for different SiH_4:NH_3 ratios.

SiH_4:NH_3	Si:N	H (%)
1:1	3.2670	34.88
1:10	0.9887	28.52
1:20	0.9115	26.68
1:50	0.8755	23.78
1:100	0.8421	23.88

obtained by Houska *et al.*[48] The SiH_4:NH_3 ratio can also influence the Si:N ratio in the film. From Table VI, we can see that Si:N ratio decreases with the increasing of NH_3 concentration in the reactant gases. This trend shows that films with ideal Si:N ratios may be obtained by carefully choosing the SiH_4:NH_3 ratios.

V. SUMMARY

In summary, we developed a new SW type interatomic potential for Si/N/H system based on first principle calculations. We employed this new potential to perform simulations of chemical vapor deposition (CVD) film growth on Si(100) substrate with SiH_4/NH_3 gas mixture. The simulations clearly revealed the details of SiN film growth and the results qualitatively agreed with the experiments. Trend of the composition analyzing the simulation results shows that silicon nitride films with ideal Si:N may be obtained by carefully choosing SiH_4:NH_3 ratios. It is demonstrated that this newly developed potential model is suitable to describe the surface reactions of the Si/N/H system and can be further used to study more complex silicon nitride film growth process such as PECVD.

ACKNOWLEDGMENTS

This work was financially supported by the National Science and Technology Major Project of China (2011ZX2403-002).

[1]J. W. Coburn and H. F. Winters, "Ion- and electron-assisted gas-surface chemistry—An important effect in plasma etching," J. Appl. Phys. **50**, 3189–3196 (1979).
[2]H. Abe, M. Yoneda, and N. Fujiwara, "Developments of plasma etching technology for fabricating semiconductor devices," Jpn. J. Appl. Phys., Part 1 **47**, 1435–1455 (2008).
[3]F. H. Stillinger and T. A. Weber, "Computer-simulation of local order in condensed phases of silicon," Phys. Rev. B **31**, 5262–5271 (1985).
[4]F. H. Stillinger and T. A. Weber, "Molecular-dynamics simulation for chemically reactive substances - fluorine," J. Chem. Phys. **88**, 5123–5133 (1988).
[5]F. H. Stillinger and T. A. Weber, "Fluorination of the dimerized Si(100) surface studied by molecular-dynamics simulation," Phys. Rev. Lett. **62**, 2144–2147 (1989).
[6]T. A. Weber and F. H. Stillinger, "Dynamical branching during fluorination of the dimerized Si(100) surface: A molecular dynamics study," J. Chem. Phys. **92**, 6239–6245 (1990).
[7]P. C. Weakliem, C. J. Wu, and E. A. Carter, "First-principles-derived dynamics of a surface reaction: Fluorine etching of Si(100)," Phys. Rev. Lett. **69**, 200–203 (1992).
[8]H. Feil, J. Dieleman, and B. J. Garrison, "Chemical sputtering of Si related to roughness formation of a Cl-passivated Si surface," J. Appl. Phys. **74**, 1303–1309 (1993).
[9]D. E. Hanson, J. D. Kress, and A. F. Voter, "An interatomic potential for reactive ion etching of Si by Cl ions," J. Chem. Phys. **110**, 5983–5988 (1999).
[10]B. W. H. van Beest, G. J. Kramer, and R. A. van Santen, "Force fields for silicas and aluminophosphates based on *ab initio* calculations," Phys. Rev. Lett. **64**, 1955–1958 (1990).
[11]G. J. Kramer, N. P. Farragher, B. W. H. van Beest, and R. A. van Santen, "Interatomic force fields for silicas, aluminophosphates, and zeolites: Derivation based on *ab initio* calculations," Phys. Rev. B **43**, 5068–5080 (1991).
[12]Z. Jiang and R. A. Brown, "Atomistic calculation of oxygen diffusivity in crystalline silicon," Phys. Rev. Lett. **74**, 2046–2049 (1995).
[13]T. Watanabe, H. Fujiwara, H. Noguchi, T. Hoshino, and I. Ohdomari, "Novel interatomic potential energy function for Si, O mixed systems," Jpn. J. Appl. Phys. **38**, L366–L369 (1999).
[14]H. Ohta and S. Hamaguchi, "Classical interatomic potentials for Si–O–F and Si–O–Cl systems," J. Chem. Phys. **115**, 6679–6690 (2001).
[15]V. V. Smirnov, A. V. Stengach, K. G. Gaynullin, V. A. Pavlovsky, S. Rauf, P. J. Stout, and P. L. G. Ventzek, "Molecular-dynamics model of energetic fluorocarbon-ion bombardment on SiO_2 I. Basic model and CF_2^+-ion etch characterization," J. Appl. Phys. **97**, 093302 (2005).
[16]V. V. Smirnov, A. V. Stengach, K. G. Gaynullin, V. A. Pavlovsky, S. Rauf, and P. L. G. Ventzek, "A molecular dynamics model for the interaction of energetic ions with SiOCH low-kappa dielectric," J. Appl. Phys. **101**, 053307 (2007).
[17]H. Ohta, A. Iwakawa, K. Eriguchi, and K. Ono, "An interatomic potential model for molecular dynamics simulation of silicon etching by Br^+-containing plasmas," J. Appl. Phys. **104**, 073302 (2008).
[18]T. Nagaoka, K. Eriguchi, K. Ono, and H. Ohta, "Classical interatomic potential model for Si/H/Br systems and its application to atomistic Si etching simulation by HBr^+," J. Appl. Phys. **105**, 023302 (2009).
[19]J. Tersoff, "New empirical model for the structural properties of silicon," Phys. Rev. Lett. **56**, 632–635 (1986).
[20]J. Tersoff, "New empirical approach for the structure and energy of covalent systems," Phys. Rev. B **37**, 6991–7000 (1988).
[21]J. Tersoff, "Empirical interatomic potential for silicon with improved elastic properties," Phys. Rev. B **38**, 9902–9905 (1988).
[22]J. Tersoff, "Empirical interatomic potential for carbon, with applications to amorphous carbon," Phys. Rev. Lett. **61**, 2879–2882 (1988).
[23]J. Tersoff, "Modeling solid-state chemistry: Interatomic potentials for multicomponent systems," Phys. Rev. B **39**, 5566–5568 (1989).
[24]D. W. Brenner, "Empirical potential for hydrocarbons for use in simulating the chemical vapor deposition of diamond films," Phys. Rev. B **42**, 9458–9471 (1990).
[25]J. Tanaka, C. F. Abrams, and D. B. Graves, "New C–F interatomic potential for molecular dynamics simulation of fluorocarbon film formation," J. Vac. Sci. Technol., A **18**, 938–945 (2000).
[26]C. F. Abrams and D. B. Graves, "Energetic ion bombardment of SiO_2 surfaces: Molecular dynamics simulations," J. Vac. Sci. Technol., A **16**, 3006–3019 (1998).
[27]L. Pizzagalli, J. Godet, J. Guénolé, S. Brochard, E. Holmstrom, K. Nordlund, and T. Albaret, "A new parametrization of the Stillinger–Weber potential for an improved description of defects and plasticity of silicon," J. Phys.: Condens. Matter **25**, 055801 (2013).
[28]Y. Lee and G. S. Hwang, "Force-matching-based parameterization of the stillinger-weber potential for thermal conduction in silicon," Phys. Rev. B **85**, 125204 (2012).
[29]H. Ohta, T. Nagaoka, K. Eriguchi, and K. Ono, "An improvement of stillinger–weber interatomic potential model for reactive ion etching simulations," Jpn. J. Appl. Phys., Part 1 **48**, 020225 (2009).
[30]G. Kresse and J. Furthmuller, "Efficiency of ab-initio total energy calculations for metals and semiconductors using a plane-wave basis set," Comput. Mater. Sci. **6**, 15 (1996).
[31]G. Kresse and J. Furthmuller, "Efficient iterative schemes for ab initio total-energy calculations using a plane-wave basis set," Phys. Rev. B **54**, 11169 (1996).
[32]J. P. Perdew, J. A. Chevary, S. H. Vosko, K. A. Jackson, M. R. Pederson, D. J. Singh, and C. Fiolhais, "Atoms, molecules, solids, and surfaces—Applications of the generalized gradient approximation for exchange and correlation," Phys. Rev. B **46**, 6671 (1992).
[33]J. P. Perdew, J. A. Chevary, S. H. Vosko, K. A. Jackson, M. R. Pederson, D. J. Singh, and C. Fiolhais, "Atoms, molecules, solids, and surfaces—Applications of the generalized gradient approximation for exchange and correlation," Phys. Rev. B **48**, 4978 (1993).

[34]D. R. Lide, *CRC Handbook of Chemistry and Physics, Internet Version 2005* (CRC Press, Boca Raton, FL, 2005), http://www.hbcpnetbase.com.
[35]F. de Brito Mota, J. F. Justo, and A. Fazzio, "Hydrogen role on the properties of amorphous silicon nitride," J. Appl. Phys. **86**, 1843–1847 (1999).
[36]E. Fattal, M. R. Radeke, G. Reynolds, and E. A. Carter, "Ab initio structure and energetics for the molecular and dissociative adsorption of nh3 on si(100)-2 1?," J. Phys. Chem. B **101**, 8658–8661 (1997).
[37]C. F. Melius and P. Ho, "Theoretical study of the thermochemistry of molecules in the silicon-nitrogen-hydrogen-fluorine system," J. Phys. Chem. **95**, 1410–1419 (1991).
[38]F. Birch, "Finite elastic strain of cubic crystals," Phys. Rev. **71**, 809–824 (1947).
[39]W. Ching, L. Ouyang, and J. D. Gale, "Full ab initio geometry optimization of all known crystalline phases of si_ {3} n_ {4}," Phys. Rev. B **61**, 8696 (2000).
[40]A. Zerr, G. Miehe, G. Serghiou, M. Schwarz, E. Kroke, R. Riedel, H. Fueß, P. Kroll, and R. Boehler, "Synthesis of cubic silicon nitride," Nature **400**, 340–342 (1999).
[41]S. Plimpton, "Fast parallel algorithms for short-range molecular dynamics," J. Comput. Phys. **117**, 1–19 (1995).
[42]Y. Widjaja and C. B. Musgrave, "*Ab initio* study of the initial growth mechanism of silicon nitride on Si(100)−(2×1) using NH_3," Phys. Rev. B **64**, 205303 (2001).
[43]O. N. Chung, H. Kim, S. Chung, and J.-Y. Koo, "Multiple adsorption configurations of NH_3 molecules on the Si(001) surface," Phys. Rev. B **73**, 033303 (2006).
[44]M. Dai, Y. Wang, J. Kwon, M. D. Halls, and Y. J. Chabal, "Nitrogen interaction with hydrogen-terminated silicon surfaces at the atomic scale," Nature Mater. **8**, 825–830 (2009).
[45]B. Xu, J. Dong, P. F. McMillan, O. Shebanova, and A. Salamat, "Equilibrium and metastable phase transitions in silicon nitride at high pressure: A first-principles and experimental study," Phys. Rev. B **84**, 014113 (2011).
[46]S. Fujita, H. Toyoshima, M. Nishihara, and A. Sasaki, "Variations of trap states and dangling bonds in cvd si3n4 layer on si substrate by nh3/sih4 ratio," J. Electron. Mater. **11**, 795–812 (1982).
[47]R. Chow, W. A. Lanford, W. Ke-Ming, and R. S. Rosler, "Hydrogen content of a variety of plasma-deposited silicon nitrides," J. Appl. Phys. **53**, 5630–5633 (1982).
[48]J. Houska, J. E. Klemberg-Sapieha, and L. Martinu, "Atom-by-atom simulations of chemical vapor deposition of nanoporous hydrogenated silicon nitride," J. Appl. Phys. **107**, 083501 (2010).